Cartan Frame Analysis of Hearts with Infarcts

Damien Goblot[1], Mihaela Pop[2], and Kaleem Siddiqi[1(✉)]

[1] School of Computer Science and Centre for Intelligent Machines, McGill University, Quebec, Canada
siddiqi@cim.mcgill.ca
[2] Department of Medical Biophysics, Sunnybrook Research Institute, University of Toronto, Toronto, Canada

Abstract. Muscle fibers in healthy hearts follow a regular geometry, with streamlines that lie along close to parallel helical curves. This regularity is disrupted in the presence of myocardial infarction which results in a loss of contractile function due to the necrosis of myocytes and the build up of collagen. However, intermediate situations also exist with partly functional surrounding border zones. The precise manner in which fiber geometry is remodeled following the occurrence of an infarct is not known. Here we demonstrate the promise of Cartan frame fitting to diffusion magnetic resonance images of the heart to address this question. We use the error of fit of these models to the first principal eigen vector of the diffusion tensor to capture the degree of local fiber coherence. The first study of its kind in application to myocardial infarction, our experiments on porcine hearts reveal measures to assess damage that are complementary to existing scalar ones, such as the apparent diffusion coefficient or the fractional anisotropy. Cartan frame fitting provides valuable additional information about local fiber geometry.

1 Introduction

In North America alone there are almost half a million sudden deaths each year due to heart defects [16]. In patients suffering from structural heart disease over 85% of the cases arise from myocardial infarction (MI). Following MI, the deposition of collagen (the main component of cardiac connective tissue) in the scar triggers a prolonged ventricular remodelling process [11]. Studies have shown that by 4 weeks after the occurrence of an infarct, mature fibrosis has replaced necrotic myocytes [3,5]. This deposition of collagen is heterogeneous due to surviving blood vessels which continue to supply oxygen to the peri-infarct area [2], resulting in a mixture of viable and necrotic cells to form a border zone (BZ), which in turn can generate lethal arrhythmias [12]. Developing non-invasive methods to characterize the BZ has been the focus of many research groups.

A common strategy is to use diffusion-weighted (DW) imaging to provide scalar parametric maps of the apparent diffusion coefficient (ADC) and the fractional anisotropy (FA), which can identify in vivo scar areas in patients with

T. Mansi et al. (Eds.): STACOM 2016, LNCS 10124, pp. 87–95, 2017.
DOI: 10.1007/978-3-319-52718-5_10

prior-infarction [15] and structural changes in infarcted porcine hearts, ex vivo [8,14]. The molecular diffusion of water molecules reflects microstructural tissue integrity and there is a gradual loss of fiber coherence in the ischemic BZ and dense scar regions due to collagen deposition. The loss in fiber coherence leads to a decrease in FA in these regions, while the deposition of collagen combined with increased extracellular spacing results in elevated ADC values. This relationship between ADC and FA is illustrated by the examples in Fig. 1, with the ADC map (top left) showing increased diffusion (yellowish tones) in the scar tissue, and the FA map showing a corresponding decrease (dark blue tones) in anisotropy (top middle) in an infarcted pig heart.

In healthy mammalian hearts myofibers are known to lie along helical curves, an arrangement that is critical for normal mechanical and electrophysiological function [4]. Numerous mathematical models for this arrangement have been proposed in the literature including [1,6,9,10]. Much less is known, however, about the manner in which heart wall myofibers rearrange in the presence of infarcts. Qualitatively, in healthy regions the fibers maintain a smoothly varying helical pattern, as revealed by tractography (Fig. 1, bottom left), while at locations affected by the infarct their geometry is much more chaotic (Fig. 1, bottom right).

Motivated by the above considerations, we propose to use the error of fit of Cartan frames to fiber orientation data from DW images as a measure of fiber orientation incoherence. We demonstrate the association of regions with a high error of fit with an infarct, while simultaneously providing parametric maps of fiber geometry in healthy tissue. We provide experimental results on several porcine hearts with infarcts and one that is healthy. As a preview of these results, Fig. 1 (top right) shows that regions of low error of fit (dark blue) are consistent with the healthy tissue, as corroborated by the ADC and FA maps. Regions with high error of fit (yellow tones) correspond well with the infarcted regions, where fiber incoherence is expected, but additionally include locations near the epithelial and endothelial linings.

2 Methods

2.1 Modeling Fiber Geometry via Connection Forms

We utilize the methods of [7] to describe the geometry of fiber orientation in the heart wall via rotations of a frame field that is fit to the DW data. Let a point $\boldsymbol{x} = \sum_i x_i \boldsymbol{e}_i \in \mathbf{R}^3$ be expressed in terms of $\boldsymbol{e}_1, \boldsymbol{e}_2, \boldsymbol{e}_3$, the natural basis for $\mathbf{R}^3$. We define a right-handed orthonormal frame field $\boldsymbol{f}_1, \boldsymbol{f}_2, \boldsymbol{f}_3 : \mathbf{R}^3 \to \mathbf{R}^3$. Each frame axis can be expressed by the rigid rotation $\boldsymbol{f}_i = \sum_j a_{ij} \boldsymbol{e}_j$, where $\boldsymbol{A} = \{a_{ij}\} \in \mathbf{R}^{3\times 3}$ is a differentiable attitude matrix such that $\boldsymbol{A}^{-1} = \boldsymbol{A}^T$. Treating $\boldsymbol{f}_i$ and $\boldsymbol{e}_j$ as symbols, we can write

$$\begin{bmatrix} \boldsymbol{f}_1 & \boldsymbol{f}_2 & \boldsymbol{f}_3 \end{bmatrix}^T = \boldsymbol{A} \begin{bmatrix} \boldsymbol{e}_1 & \boldsymbol{e}_2 & \boldsymbol{e}_3 \end{bmatrix}^T. \tag{1}$$

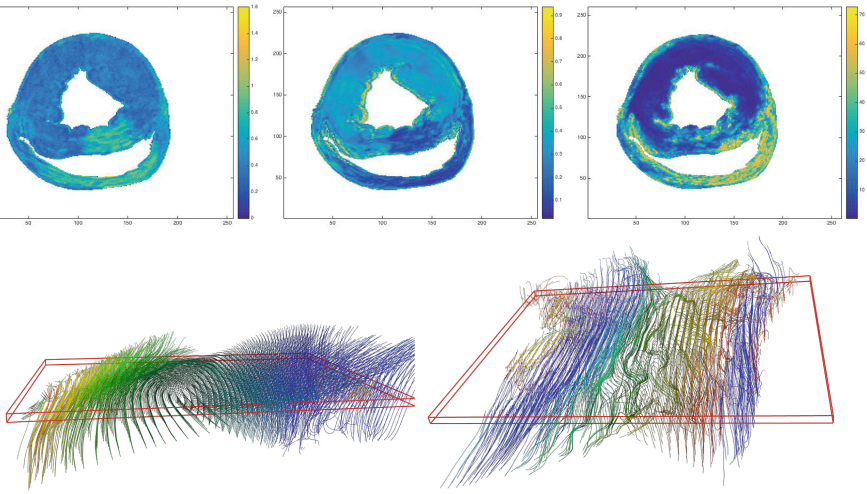

Fig. 1. Ex vivo diffusion imaging of a pig heart. Top: The ADC map (left), with regions of high diffusion shown in shades of yellow, the FA map (middle), with regions of low FA shown in darker blue and the error of fit in degrees generated by fitting 1-forms (right). Bottom: Streamline tractography seeded in a healthy region of the LV wall (left) and in a region of the septum affected by the infarct (right). Both tractography results are visualized from a circumferential direction. See text for a discussion. (Color figure online)

Since each $\boldsymbol{e}_i$ is constant, the differential geometry of the frame field is completely characterized by $\boldsymbol{A}$. Taking the exterior derivative on both sides, we have

$$\mathrm{d}\left[\boldsymbol{f}_1\ \boldsymbol{f}_2\ \boldsymbol{f}_3\right]^T = (\mathrm{d}\boldsymbol{A})\,\boldsymbol{A}^{-1}\left[\boldsymbol{f}_1\ \boldsymbol{f}_2\ \boldsymbol{f}_3\right]^T = \boldsymbol{C}\left[\boldsymbol{f}_1\ \boldsymbol{f}_2\ \boldsymbol{f}_3\right]^T, \tag{2}$$

where d denotes the exterior derivative, and $\boldsymbol{C} = (\mathrm{d}\boldsymbol{A})\,\boldsymbol{A}^{-1} = \{c_{ij}\} \in \mathbf{R}^{3\times 3}$ is the Maurer-Cartan matrix of connection forms c_{ij}. Writing $\boldsymbol{f}_i$ as symbols, (2) is to be understood as $\mathrm{d}\boldsymbol{f}_i = \sum_j c_{ij}\boldsymbol{f}_j$. The Maurer-Cartan matrix is skew symmetric with zeros as diagonal entries so there are at most 3 independent, non-zero 1-forms: c_{12}, c_{13}, and c_{23}. 1-forms operate on vectors through *contraction*, written as $\mathrm{d}w\langle\boldsymbol{v}\rangle \in \mathbf{R}$ for a general 1-form $\mathrm{d}w = \sum_i w_i \mathrm{d}\boldsymbol{e}_i$ and vector $\boldsymbol{v}$ on $\mathbf{R}^3$, which yields $\mathrm{d}w\langle\boldsymbol{v}\rangle = \sum_i w_i \mathrm{d}\boldsymbol{e}_i\langle\sum_j v_j\boldsymbol{e}_j\rangle = \sum_i w_i v_i$, since $\mathrm{d}\boldsymbol{e}_i\langle\boldsymbol{e}_j\rangle = \delta_{ij}$, where δ_{ij} is the Kronecker delta. It turns out that the space of linear models for smoothly varying frame fields is parametrized by the 1-forms c_{ij}. Since only 3 unique non-zero combinations of c_{ij} are possible, there are in total 9 connection parameters c_{ijk}. These coefficients express the rate of turn of the frame vector $\boldsymbol{f}_i$ towards $\boldsymbol{f}_j$ when $\boldsymbol{x}$ moves in the direction $\boldsymbol{f}_k$. With $\boldsymbol{f}_1$ taken as the local orientation of a fiber and $\boldsymbol{f}_3$ taken to be the component of the heart wall normal orthogonal to $\boldsymbol{f}_1$, Fig. 2 illustrates the connection parameter c_{123} describing the rotation of fibers in the direction of a transmural penetration of the heart wall.

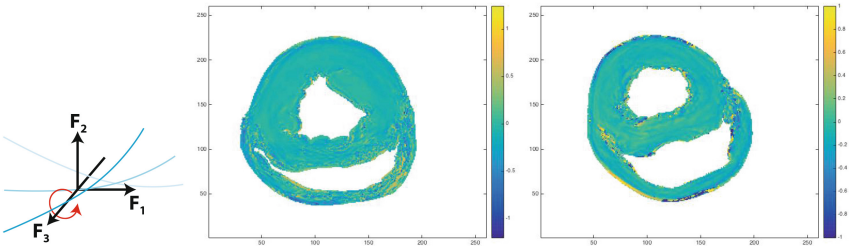

(a) c_{123} (b) c_{123} (infarct) (c) c_{123} (healthy)

Fig. 2. Connection forms measure the local rotations of the frame axes $\boldsymbol{f}_1, \boldsymbol{f}_2, \boldsymbol{f}_3$. Here we focus on the contraction of the 1-form c_{12} on the frame axis $\boldsymbol{f}_3$ and compare its values in a short axis slice of a pig heart with an infarct (middle) with those in a short axis slice from a healthy pig heart (right). See text for a discussion.

Cartan frame fitting applies to smoothly rotating frame fields. In the presence of infarcts fiber orientation coherence is lost and the fitting errors using this method increase (Fig. 1 middle left). We shall exploit this association of frame field fitting error with fiber incoherence.

2.2 Cartan Frame Fitting and Error Analysis

At each voxel we use the first principal eigen vector of a diffusion tensor reconstruction to represent the fiber orientation as $\boldsymbol{f}_1$. We then estimate the heart wall normal as the gradient of the distance function to the boundary of the myocardium and take its component orthogonal to $\boldsymbol{f}_1$ to be $\boldsymbol{f}_3$. $\boldsymbol{f}_2$ is then taken to be their cross product. To find the 9 connection parameters at each voxel we use Nelder-Mead optimization to minimize a fitting energy. This energy is defined at each voxel as the average of the angle between the measured orientation from DW data at each voxel in a local neighborhood and that given by rotating the frame field by a particular set of connections. Once this method has converged to a set of connection parameters the fitting error at the voxel is taken to be this average angular error between the model and the data.

2.3 Pig Hearts

In this study we used healthy and infarcted porcine hearts. The hearts were freshly excised, suspended in a plexiglass phantom filled with fluorinert to eliminate artifacts and placed in an MR head coil for ex vivo imaging. All DW-MR studies were performed on a dedicated 1.5T GE Signa Excite scanner using a custom FSE pulse sequence. We used the following MR parameters: TE = 35 ms, TR = 700 ms, echo train length = 2, b value = 0 for the un-weighted MR images and b value = 500 s/mm^2 when the 7 diffusion gradients were applied, respectively. We used a 256×256 k-space, FOV = 10–16 cm and a slice thickness of 1.2 mm, yielding a sub-millimetric voxel size. From each heart, select samples

containing an infarct were cut to align with the short-axis view of the MR images and prepared for histopathology to confirm the collagen deposition in the infarct area. The details of the methods used to generate the chronic infarcts are presented in [8].

3 Results and Discussion

Reconstruction and Filtering. We used an established Rician smoothing method to reduce noise in the diffusion images [13]. The parameters for this non-local filtering method guided by voxel to voxel similarity were tuned to prevent over-smoothing. We used the publicly available MedInria software to carry out the filtering, and to then reconstruct the diffusion tensor from the raw diffusion weighted scans, from which fiber orientations were extracted as the first principal eigen vector. We used a threshold on the FA map as a mask to restrict further processing.

Comparison with Histology. We first applied a combination of linear and non-linear registration transformations using functions readily available in Matlab, in particular *imregtform*, to align histological slices to their corresponding DW slices. We then compared ADC maps with Cartan frame fitting-based error of fit maps. Supplementing the earlier results in Fig. 1, Fig. 3 shows the ADC map (left) the error of fit map in degrees (middle) and a histology image (right) for a different slice of the dataset in Fig. 1 (top row) and for a selected region from a different infarcted pig heart (middle row). The histology images show intact myocytes in the normal tissue and altered tissue microstructure in the infarcted zones. As depicted by the Masson Trichrome stain, the ischemic border zones (BZ) had collagen fibrils interdigitated between viable myocytes. In the dense scar areas, necrotic myocytes were completely replaced by mature fibrosis (the final product of collagen degradation), resulting in a loss of myocardial anisotropy. The bottom row shows tractography results for these cases. As before there is qualitatively good agreement between regions with high ADC values and regions with high error of fit (yellowish tones). The results also show regions of viable tissue (greenish tones in the error of fit maps) within the infarcted areas, which is corroborated by the tractography results. In particular, there appear to be regions of coherent fibers within the septum of the first heart (third row left) and the LV wall of the second heart (third row right and bottom row left).

Quantitative Results. Given the association between ADC and our error of frame fit, it is natural to compare these measures quantitatively throughout the myocardium. We did so for the 5 infarcted porcine hearts we analyzed by computing Dice coefficients to describe the overlap, in the following manner. For the same heart let A be the set of voxels with ADC value >0.6 and let B be the set of voxels with error of fit $>15°$. The ADC threshold is chosen based on results in [8] which demonstrate the mean ADC value of normal tissue for these DW scans to be below 0.5 with the mean value of border zone or scar tissue regions being above 0.6. The error of fit threshold was chosen by empirical

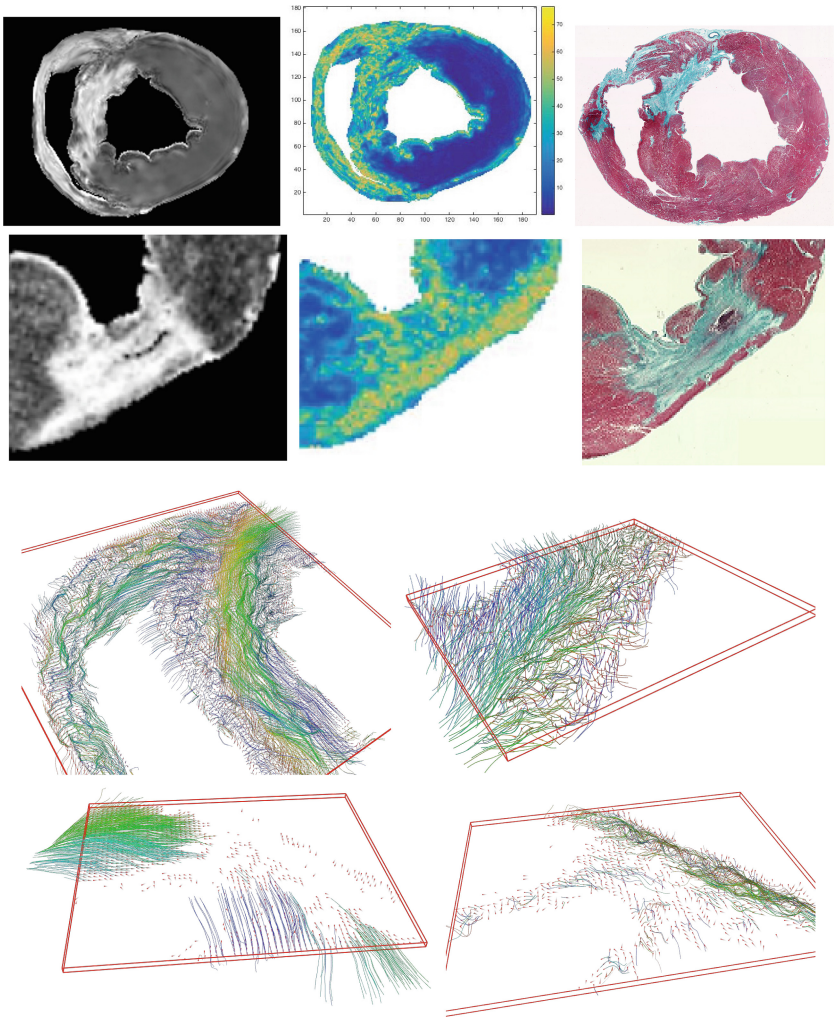

Fig. 3. We now register the histology to the DW images and show the ADC map (left) the error of fit (middle) and the registered histological image (right) for a different slice of the dataset in Fig. 1 (top row) and for a zoomed-in region of a different pig heart with an infarct (second row). The corresponding tractography results are shown in the third row. The bottom row shows tractography for the second case while seeding separately from locations with low error of fit (left) and high error of fit (right). (Color figure online)

considerations, but modest changes to it did not significantly alter the standard Dice coefficient, computed as $A \cap B/A \cup B$, or a modified coefficient computed as $A \cap B/A$. These results, shown in Table 1 (left), demonstrate that typically over 80% of the locations with increased diffusion also yield a high error of fit

Table 1. Dice coefficients between voxels A with high ADC (>0.6) and voxels B with high error of fit (>15) degrees.

Pig	$A \cap B/A \cup B$	$A \cap B/A$
Pig 2	.40	.80
Pig 4	.43	.89
Pig 5	.47	.76
Pig 6	.46	.87
Pig 7	.27	.94

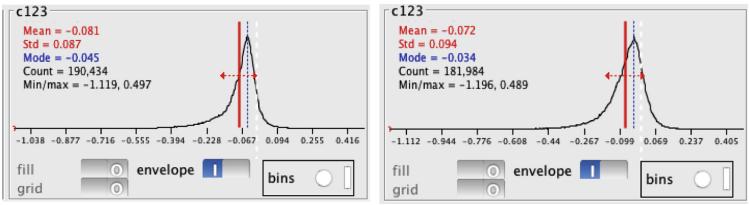

Fig. 4. Histograms of the c_{123} connection parameter over all voxels with low error of fit in an infarcted heart (left) and over all voxels in a healthy heart (right).

using our frame fitting method, due to the loss of geometric coherence of fiber orientations. However there are additional locations where fiber orientations are not smooth, typically at the linings of the heart wall, or near the edges of a collapsing and narrow right ventricle. Such regions are not picked up by the ADC or FA measures likely because there is no increase in collagen or loss in anisotropy there. As such, we hypothesize that these are regions where the fiber orientation is simply distinct from that of neighboring locations, i.e., it does not form a coherent pattern.

We also present histograms in Fig. 4 to compare the c_{123} connection parameter in the infarcted pig heart of Fig. 1, but restricted to locations where the error of fit is low, with the c_{123} parameter for the healthy heart. This connection parameter attains by far the largest values in healthy hearts, because it relates to the transmural turning of fibers from outer wall to inner wall. The histograms have very similar distributions and mean values in voxel units, suggesting that in regions away from the infarct, the fiber geometry remains similar to that of a healthy heart.

4 Conclusion

We have demonstrated the use of Cartan frame fitting to characterize collagenous fibrosis and to provide quantitative assessment of fiber coherence in the presence of structural heart disease, using high resolution DW imaging in infarcted porcine hearts. Although our Cartan frame fits were applied to a relatively small sample

size of 5 diseased hearts and 1 healthy one, the results are consistent and the method holds promise for the measurement of fiber coherence in dense scar areas and more importantly in the BZ, where the substrate of lethal arrhythmia resides. In future work we plan to carry out this analysis using in vivo DW MR data, in an effort to integrate our frame fitting methods into clinical platforms for better differential diagnosis. We also hope to provide personalized estimates of fiber directions for use in mathematical models for in silico prediction of electro-mechanical function in hearts with infarcts.

References

1. Bayer, J., Blake, R., Plank, G., Trayanova, N.: A novel rule-based algorithm for assigning myocardial fiber orientation to computational heart models. Ann. Biomed. Eng. **40**(10), 2243–2254 (2012)
2. de Baker, J.M., Coronel, R., Tasseron, S., Wilde, A.A., Opthof, T., Janse, M.J., van Capelle, F.J., Becker, A.E., Jambroes, G.: Ventricular tachyrdia in the infarcted, langendorff-perfused human heart: role of the arrangement of surviving cardiac fibers. J. Am. Coll. Cardiol. **15**(7), 1594–1607 (1990)
3. Holmes, J., Yamashita, H., Waldman, L., Covell, J.: Scar remodeling and transmural deformation after infarction in the pig. Circulation **90**(1), 411–420 (1994)
4. Horowitz, A., Perl, M., Sideman, S.: Geodesics as a mechanically optimal fiber geometry for the left ventricle. Basic. Res. Cardiol. **88**(Suppl 2), 67–74 (1993)
5. McCormick, R.J., Musch, T.I., Bergman, B.C., Thomas, D.P.: Regional differences in LV collagen accumulation and mature cross-linking after myocardial infarction in rats. Am. J. Physiol. Heart Circulatory Physiol. **266**(1), H354–H359 (1994)
6. Peskin, C.S.: Fiber architecture of the left ventricular wall: an asymptotic analysis. Commun. Pure Appl. Math. **42**(1), 79–113 (1989)
7. Piuze, E., Sporring, J., Siddiqi, K.: Maurer-cartan forms for fields on surfaces: application to heart fiber geometry. IEEE Trans. Pattern Anal. Mach. Intell. **37**(12), 2492–2504 (2015)
8. Pop, M., Ghugre, N.R., Ramanan, V., Morikawa, L., Stanisz, G., Dick, A.J., Wright, G.A.: Quantification of fibrosis in infarcted swine hearts by ex vivo late gadolinium-enhancement and diffusion-weighted MRI methods. Phys. Med. Biol. **58**(15), 5009 (2013)
9. Savadjiev, P., Strijkers, G.J., Bakermans, A.J., Piuze, E., Zucker, S.W., Siddiqi, K.: Heart wall myofibers are arranged in minimal surfaces to optimize organ function. Proc. Natl. Acad. Sci. **109**(24), 9248–9253 (2012)
10. Streeter, D.D.: Gross morphology and fiber geometry of the heart. In: Berne, R.M., Sperelakis, N. (eds.) Handbook of Physiology, Section 2. The Heart, pp. 61–112. Williams and Wilkins, New York (1979)
11. Swynghedauw, B.: Molecular mechanisms of myocardial remodeling. Physiol. Rev. **79**(1), 215–262 (1999)
12. Ursell, P.C., Gardner, P.I., Albala, A., Fenoglio, J., Wit, A.L.: Structural and electrophysiological changes in the epicardial border zone of canine myocardial infarcts during infarct healing. Circ. Res. **56**(3), 436–451 (1985)
13. Wiest-Daesslé, N., Prima, S., Coupé, P., Morrissey, S.P., Barillot, C.: Rician noise removal by non-local means filtering for low signal-to-noise ratio MRI: applications to DT-MRI. In: Metaxas, D., Axel, L., Fichtinger, G., Székely, G. (eds.) MICCAI 2008. LNCS, vol. 5242, pp. 171–179. Springer, Heidelberg (2008). doi:10.1007/978-3-540-85990-1_21

14. Wu, E.X., Wu, Y., Nicholls, J.M., Wang, J., Liao, S., Zhu, S., Lau, C.-P., Tse, H.-F.: MR diffusion tensor imaging study of postinfarct myocardium structural remodeling in a porcine model. Magn. Reson. Med. **58**(4), 687–695 (2007)
15. Wu, M.-T., Su, M.-Y.M., Huang, Y.-L., Chiou, K.-R., Yang, P., Pan, H.-B., Reese, T.G., Wedeen, V.J., Tseng, W.-Y.I.: Sequential changes of myocardial microstructure in patients postmyocardial infarction by diffusion-tensor cardiac mr correlation with left ventricular structure and function. Circ. Cardiovasc. Imaging **2**(1), 32–40 (2009)
16. Zipes, D.P.: Epidemiology and mechanisms of sudden cardiac death. Can. J. Cardiol. **21**, 37A–40A (2005)